

Mechanism and Applications of Electrical Stimulation Disturbance on Motoneuron Excitability Studied Using Flexible Intramuscular Electrode

Jiahui Wang, Hao Wang, and Chengkuo Lee*

Wearable and implantable devices are irreplaceable components in the modern healthcare system. Electrical stimulation on the nervous and neuromuscular system, as a way of therapeutic interventions, has been widely applied to people with neurological disorders and neuromuscular disabilities. The conventional way to study electrical stimulation on the skeletal muscle employs single-channel wire electrodes, which have limited capability to explore the complicated motoneuron distribution in muscle tissue. Here, a microfabricated flexible multiple-channel intramuscular electrode is presented, which enables the study of electrical stimulation using electrode sites of different spatial arrangements with respect to the motoneuron distribution. Observations are reported on slow disturbance on motoneuron excitability induced by large-distance electrodes targeting at the end motor nerves, as well as fast disturbance induced by small-distance electrodes targeting at the main motor nerve trunk. The phenomena of slow and fast disturbance have different potential applications in the field of neuromodulation. In the case of slow disturbance, force output is predictable and shows gradual change, which is suitable for accurately controlled functional electrical stimulation (FES). For fast disturbance, the disappearance of force output opens the possibility for muscle conduction block applications, which can be used for treatment of muscle sparsity by blocking the involuntary motor intentions.

1. Introduction

The explosive demand for healthcare service in modern society has prompted the recent vast progress in wearable and implantable devices,^[1] in terms of both novel material

Dr. J. Wang, Dr. H. Wang, Prof. C. Lee
Department of Electrical & Computer Engineering
National University of Singapore
4 Engineering Drive 3, Singapore 117576, Singapore
E-mail: elelc@nus.edu.sg

Dr. J. Wang, Prof. C. Lee
Singapore Institute for Neurotechnology (SINAPSE)
National University of Singapore
28 Medical Drive, #05-COR, Singapore 117456, Singapore

Dr. J. Wang, Dr. H. Wang, Prof. C. Lee
Center for Intelligent Sensors and MEMS
National University of Singapore
4 Engineering Drive 3, Singapore 117576, Singapore

 The ORCID identification number(s) for the author(s) of this article can be found under <https://doi.org/10.1002/adbi.201800281>.

DOI: 10.1002/adbi.201800281

development^[2–5] and new technology applications.^[6–8] Together with the emerging Internet of Things (IoT) and Artificial Intelligence (AI) technology, wearable and implantable devices are becoming an irreplaceable component in the modern healthcare system,^[9,10] as shown in **Figure 1A**. Various wearable sensing platforms have been applied in human vital signs monitoring,^[11,12] including body temperature,^[13] heart rate,^[14] respiration rate,^[15] blood pressure,^[16] and sweat electrolyte.^[17] These wearable sensing platforms provide cost-efficient solutions for long-term fitness monitoring and medical diagnostics purposes.^[18–20]

Moving forward, when certain diseases have occurred, and mere healthcare monitoring is not enough, therapeutic interventions are required. Implantable devices have empowered novel therapeutic interventions. To selectively activate certain excitable cells, integrated optogenetics devices are implanted in the muscle,^[21] peripheral nerves,^[22] and cortex^[23] to deliver light therapy. To mechanically induce tissue contraction in disordered

organs, actuators are applied on the heart^[24] and bladder.^[25] To improve drug diffusion, small-scale drug delivery systems are developed.^[26,27] One of the most popular way to deliver therapeutic interventions is to electrically stimulate the nervous system. Well-established treatments include deep-brain stimulation for Parkinson's disease,^[28] cochlear implants for hearing loss,^[29] visual prosthetics,^[30] and brain-machine interfaces for movement restoration.^[31–33] In addition, emerging energy harvester technologies have enabled direct electrical stimulation on neural tissues for self-powered electrical stimulation to relieve the power supply problem for chronic implantable devices.^[34,35]

Dating back to 1770, Luigi Galvani first discovered bioelectricity as he made a frog muscle twitch by accidentally creating a battery from surgical instruments.^[36] Ever since then, people have been exploring to deliver electrical stimulation as therapeutic interventions. However, as an external intervention method, electrical stimulation is essentially different from natural action potentials. In voluntarily controlled movements, motor intentions originated from the cortex travel along individual motor axons to control various skeletal muscles.^[37] One

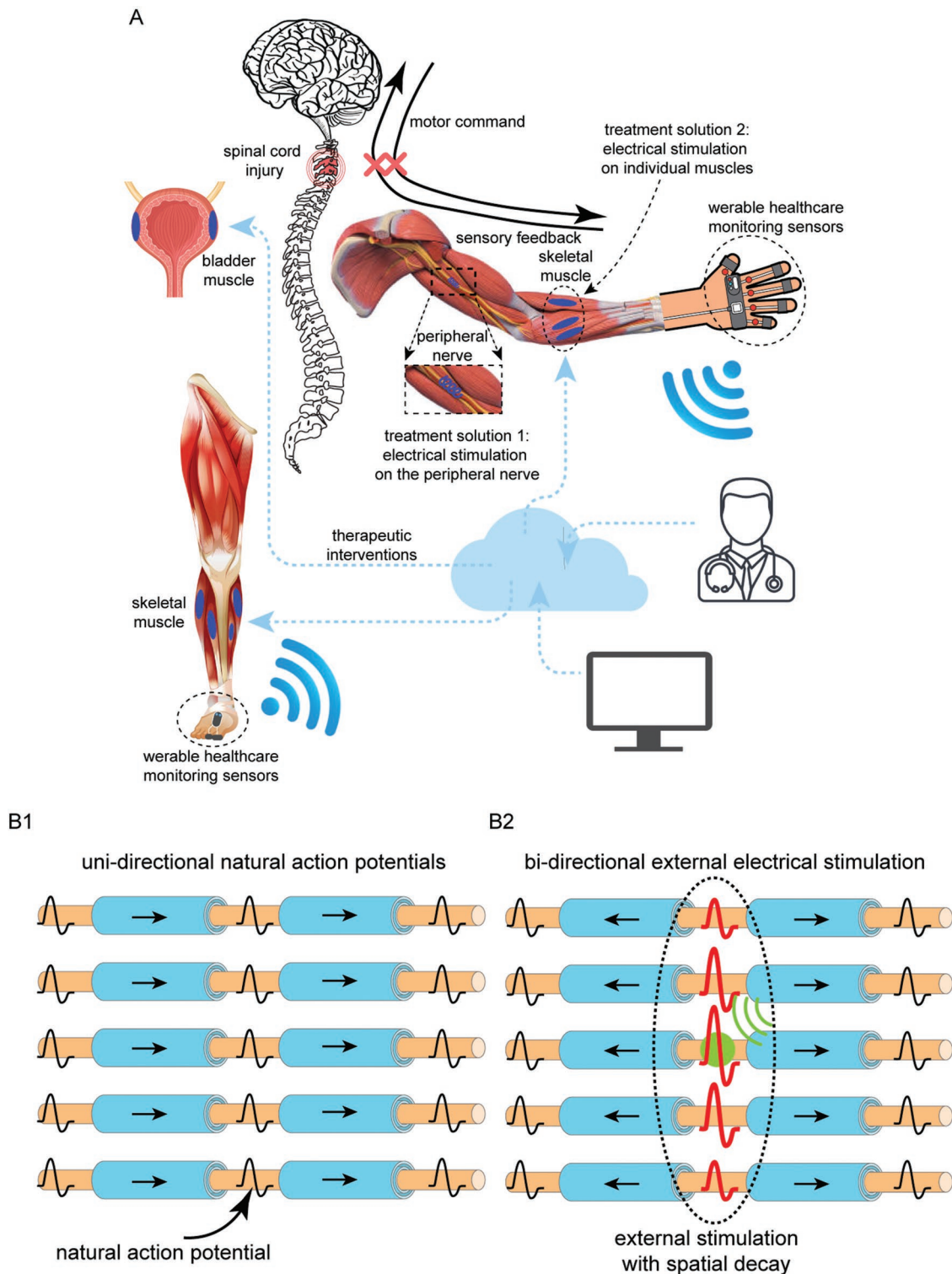


Figure 1. A) Schematic illustration of healthcare system. B1) Unidirectional transmission of natural action potentials. Action potentials are sequentially evoked on the node of Ranvier. B2) Bidirectional transmission of action potentials evoked by external electrical stimulation.

action potential will sequentially evoke the following action potential on the next node of Ranvier,^[38] so that this action potential can be relayed unidirectionally along the motoneuron axon (Figure 1B1). For electrical stimulation, transmembrane electric

field resulting from electrode–tissue interaction opens voltage-gated ion channels to initiate bidirectional action potentials that transmit on the neuron fibers (Figure 1B2). Different from natural action potentials, external electrical stimulation may

not only initiate action potentials, but also distort ion distribution by lingering on after the ion channels open. Due to the spatial decay of electric field resulting from electrode–tissue interaction,^[39] the disturbance on neuron excitability varies with respect to the distance between the affected neuron and the stimulation electrodes. The largest disturbance occurs to the neurons located close to the stimulation electrodes.

Functional electrical stimulation (FES) aims at recovering functional movements to patients suffering from stroke or spinal cord injury. To recover the disconnected communication between the cortex and skeletal muscles, implantable devices are employed to convey the efferent motor commands^[40] and afferent sensory information.^[41] To achieve skeletal muscle movement control, implantable devices target the peripheral nerves^[42] or the skeletal muscles^[43] to deliver electrical stimulation. The peripheral nerves are small in size, and they are made up of several nerve fascicles holding hundreds of nerve fibers. As an example, the human median nerve trunk, which has around 20 nerve fascicles (with an average area of 0.16 mm²), holds 20 000 axons.^[44] Considering the small diameter of the peripheral nerve and the large number of nerve fibers, selective activation of certain nerve fibers innervating a specific skeletal muscle requires complicated mapping.^[45] Instead of targeting the small-diameter peripheral nerves for movement control, an alternative solution is to directly target individual skeletal muscles, as has been routinely used for clinical applications.^[45]

The development of muscle electrodes has lagged behind other fast-developing fields in implantable devices. Even recent implantable muscle stimulation systems still employ single-channel manually prepared insulating wires with small openings for charge delivery.^[46–48] The single-channel design limits the capability of these systems to explore complicated control over the skeletal muscle. The available microfabricated multiple-channel muscle stimulation electrodes include both epimysial and intramuscular electrodes.^[49,50] The epimysial electrodes activate motoneurons distributed in the muscle tissue through poorly conductive epimysium structure, and thus suffer from low power efficiency. In addition, the epimysial electrodes cannot selectively activate motoneurons located deep in the muscle tissue, as electric field generated by the epimysial electrodes tends to spread out in the tissue. Thus, to achieve better power efficiency and selectivity, we choose to develop a microfabricated multiple-channel intramuscular electrode, to further explore the electrical stimulation disturbance on the muscle tissue.

There has been emerging interest in using flexible electrodes to interface with neural tissues because they can conform well to delicate tissues and biological structures. Due to the conformability to biological structures, these flexible electrodes are applied to the surface of cortex,^[51] the peripheral nerves,^[51] and organs,^[52] to stimulate and record neural signals. In addition, due to the flexibility rendered by the electrodes, they can deform to accommodate movements of neural tissues and biological structures and be used to target intracortical^[53] and intrafascicular^[54] tissue.

In this study, we will demonstrate how a flexible multiple-channel intramuscular electrode can be used to explore various electrical control of the skeletal muscles. Here, we explore the spatial interaction between the stimulation electrodes and the

tissue, and we discover slow and fast disturbance phenomena when targeting at the main motor nerve trunk and the end motor nerves. We then investigate the mechanism and potential applications of both slow disturbance (abrupt change of the measured force output) and fast disturbance (gradual change of the measured force output).

2. Results

2.1. Electrode Structural Design and Implantation

Two types of excitable cells exist in the muscle tissue, namely motoneurons and muscle fibers. Since the stimulation threshold for motoneurons is much lower than muscle fibers, motoneurons are excited to control muscle fibers during neuromuscular electrical stimulation. Thus, motoneuron distribution in the muscle tissue determines how we can explore the spatial arrangement of the stimulation electrodes. The motor nerve forms a tree-structure distribution in the skeletal muscle,^[54] as it keeps branching into smaller nerves on its way into the muscle to innervate muscle fibers on the midpoint.^[55,56] We speculate that electrical stimulation targeting at the main nerve trunk (before the motor nerve starts branching) and the end motor nerves (the small nerves that motor nerve branches into) will have different stimulation effects. When stimulation electrodes are close to the main nerve trunk, electrical stimulation tends to induce synchronized disturbance on all motoneurons and results in abrupt change of the force output. While for stimulation electrodes targeting at widely distributed end nerves, electrical stimulation can uniformly exert disturbance on each end nerve and results in gradual change of the force output.

To test our speculation about different stimulation effects on the tree-structure motor nerve in the muscle tissue, we design a flexible two-sided multiple-channel intramuscular electrode. **Figure 2A** shows the structural design of the electrode, which consists of two strip-like substrates connected in the midpoint. Six electrode sites uniformly distribute on each strip-like substrate. Before implantation, the two strip-like substrates are folded from the midpoint, forming a two-sided electrode with six electrode sites facing outward on each side. Such a two-sided structure facilitates easy *in vivo* implantation, as a suture wire can be used to pull the folded two-sided electrode into the skeletal muscle belly. Microelectromechanical Systems (MEMS) fabrication technology enables densely integrated multiple-channel electrode sites, so that different electrode sites can be chosen to explore the spatial distribution of the motor nerve. After sutured into the skeletal muscle belly, the flexible intramuscular electrode may intersect with the tree-structure motor nerve with different angles, as shown in **Figure 2B**. Any two electrode sites can be chosen to deliver stimulation current, and thus the flexible intramuscular electrode can selectively target the main nerve trunk or the end nerves. In addition, as comparison to the flexible intramuscular electrode, two stainless-steel wires are sutured on the same muscle near the tendons, to serve as large-distance stimulation electrodes that do not intersect with the motor nerves. These stainless-steel wires are encapsulated, with only a short section of 1 mm length exposed to contact muscle tissue for current delivery.

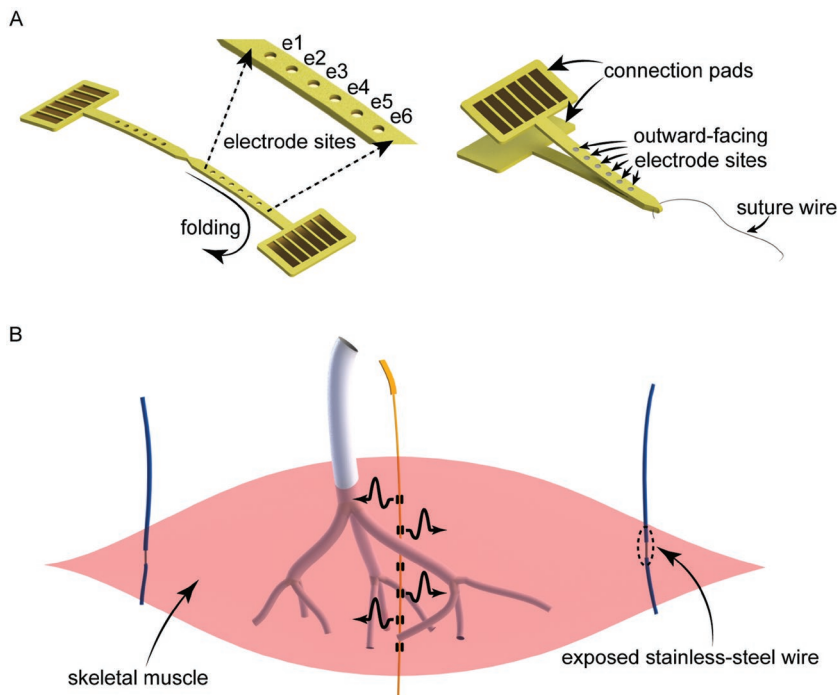


Figure 2. Illustration of electrode design and implantation in the muscle tissue. A) The flexible electrode consists of two strip-like structures, with six electrode sites distributed on each side. The strip-like structures are folded from the midpoint, and a suture wire is used to pull the electrode into the muscle belly. B) Electrode implantation and motoneuron distribution. Motor nerve innervates muscle fiber near the midpoint and branches into smaller nerves on its way into the muscle. The flexible intramuscular electrode is sutured into the muscle belly, and may intersect with motor nerve at the main trunk or the widely distributed end nerves. In addition, two stainless steel wires are sutured near the tendons of the muscle and will not directly intersect with the motor nerve.

2.2. In Vivo Experiment Setup and Stimulation Protocol

Since the tibialis anterior (TA) muscle is the most accessible skeletal muscle in the rat, we chose it to explore neuromodulation using the flexible intramuscular electrode. In addition, the contraction of the TA muscle leads to forward kicking of the leg, and the generated force output is measurable for stimulation strength quantification. The in vivo experiment setup is shown in Figure 3A. The anesthetized rat was laid on a stand, with the left leg freely suspended on one side of the stand. The detailed implantation of the flexible intramuscular electrode is shown in Figure 3B. After the flexible intramuscular electrode and two stainless steel wires were implanted in the TA muscle, the skin was sutured back. Any two electrode sites on the flexible intramuscular electrode were connected to the positive and negative terminals of the stimulator, to form a bipolar electrical stimulation configuration. When electrical stimulation was applied, the freely suspended left leg would kick forward, pulling a force gauge tied to the ankle. In this way, the electrical stimulation strength was quantized as measured force output.

Unlike metal conductor, the biological tissues show unstable impedance. Instead of having freely moving electrons as in metal conductor, the biological tissues rely on charged ions to conduct electricity. In addition, the complicated biological composites distributed in the muscle tissue, including extracellular medium,

muscle fibers, and motoneurons, also affect tissue impedance. Thus, to eliminate the biological tissue impedance fluctuation and achieve stable charge injection, current-controlled electrical stimulation was used. Since the available commercial stimulator has limited capability to generate the current stimulation waveform with the controllable parameters, we chose to customize the current stimulation waveform. Figure 3C shows the customized control loop to generate the desired current stimulation waveform. Matlab program running on a computer controls a data acquisition (DAQ) to generate voltage stimulation waveform, which is then used to control a commercial stimulator to generate the desired current stimulation waveform. Figure 3D shows the current stimulation waveform used for neuromodulation in this study. Every 1 s, a train of 10 sinewave pulses is delivered. Among the 10 sinewave pulses, one sinewave is delivered every 16.7 ms. The duration of each sinewave pulse ranges from 1000 μ s (in correspondence to 1 kHz stimulation) to 100 μ s (in correspondence to 10 kHz stimulation). Both positive-first and negative-first biphasic sinewave pulses were tested.

2.3. Observations of Fast and Slow Disturbance on Motoneuron Excitability

Two force profiles measured from the same subject, using different electrode sites on the flexible intramuscular electrode and the two stainless-steel wires respectively, are shown in Figure 4. Figure 4 shows the force profiles measured using positive-first biphasic sinewave stimulation. The force profile measured using e2 and e5 on the flexible intramuscular electrode shows abrupt decrease and increase (Figure 4A). The force profile measured using the two stainless-steel wires (Figure 4B) is stable with gradual change. In Figure 4A, although the electrical stimulation was continuously delivered to the muscle throughout the 90 s stimulation trial, no force output could be measured after 50 s. To test whether the disappearance of force output was caused by electrode failure, e2 and e5 electrode sites were used again to deliver the same positive-first biphasic stimulation after half an hour resting and induced large force output indicating that e2 and e5 were well functional (Figure S2C, Supporting Information). To account for the force disappearance in Figure 4A, the possibility of electrode failure was eliminated. Thus, the abrupt change of force output in Figure 4A was caused by motoneuron excitability change.

Up to this point, we have shown on the same subject that stimulation electrodes of different spatial arrangement generate force profile with abrupt change (Figure 4A) as well as force profiles with gradual change (Figure 4B). Then, the question arises, why stimulation electrodes of different spatial arrangement will generate such different force profiles. To address this question, we need to refer back to the spatial arrangement

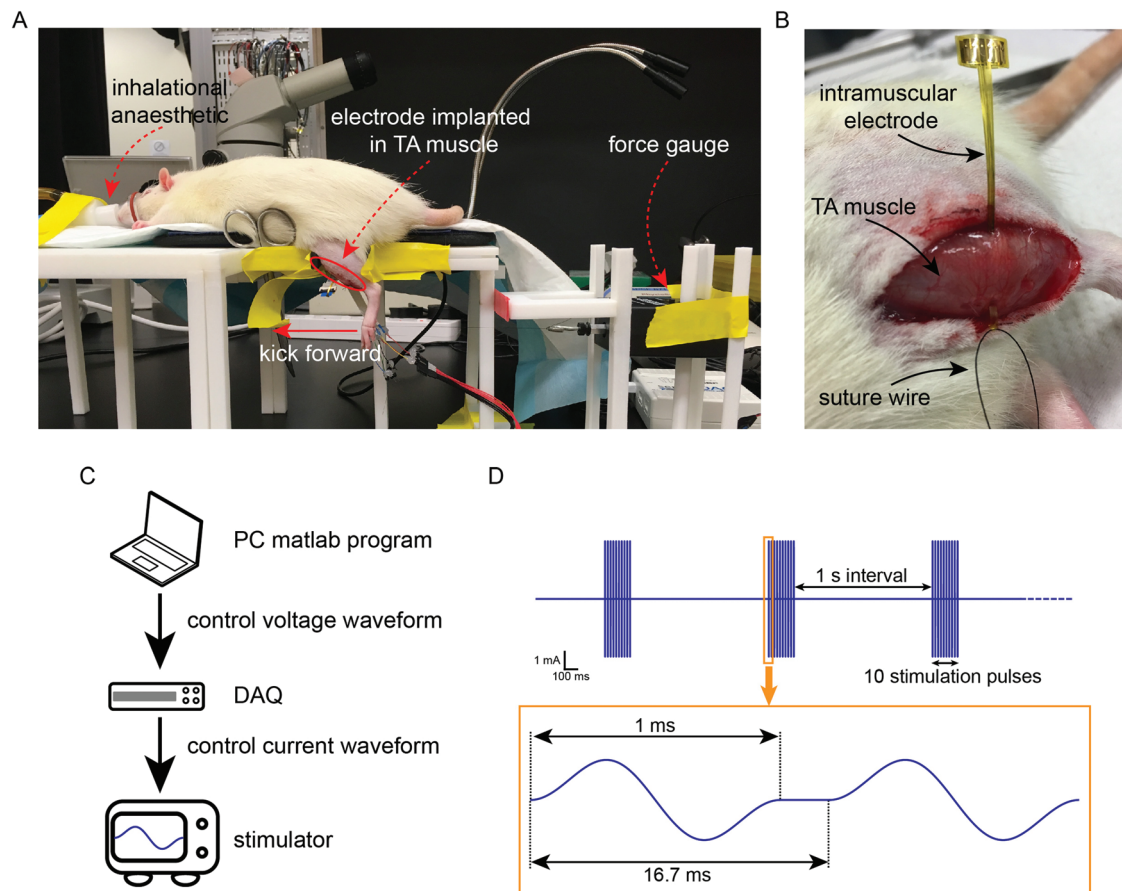


Figure 3. Experiment setup and stimulation waveform. A) Experiment setup. The anesthetized rat lies on a stand. When stimulation is delivered to the tibialis anterior (TA) muscle, the stimulated leg kicks forward, pulling the force gauge through a wire tied to the ankle. B) Picture of flexible intramuscular electrode implantation. C) The control loop to generate current stimulation waveform. D) Stimulation waveform. Every 1 s, a train of 10 sinewave pulses are delivered. Among the 10 sinewave pulses, one sinewave pulse is delivered every 16.7 ms. Every sinewave pulse lasts for 1 ms (for 1 kHz sinewave stimulation).

of the stimulation electrodes with respect to motoneuron distribution in the muscle tissue, as illustrated in Figure 2B. The flexible intramuscular electrode is sutured in the muscle belly, and it will intersect with the tree-structure distributed motoneurons. Depending on the intersection angle, some electrode sites on the flexible intramuscular electrode may stimulate the main nerve trunk, while some electrode sites may stimulate the end nerves. Localized stimulation can be achieved using this flexible intramuscular electrode due to the small separation distance in between the electrode sites. In contrast, the two stainless steel wires are sutured near the tendons of the TA muscle, and electric field will spread out to stimulation motoneurons distributed in a large area. When the main nerve trunk is electrically stimulated, since all the motoneurons are closely packed together in the main nerve trunk, these motoneurons will experience synchronized voltage waveforms of similar shape, to induce synchronized disturbance on neuron excitability, as shown in Figure 4A. When the end nerves are electrically stimulated, the end nerves distributed in a large area will experience voltage waveforms of different amplitude and polarity, which is caused by the spatial decay of electric field. Electrical stimulation of the end nerves induces gradual change of force output, as shown in Figure 4B.

Here, we define fast disturbance as synchronized disturbance on all motoneurons in the main nerve trunk, which induces force output with abrupt increase and decrease, as shown in Figure 4A. In addition, we define slow disturbance as uniform disturbance on widely distributed end motor nerves, which induces force output with gradual change, as shown in Figure 4B. In the following sessions, we will investigate the characterization of both slow and fast disturbance, as well as their applications in the field of skeletal muscle neuromodulation.

2.4. Characterization of Slow Disturbance on Motoneuron Excitability

Predictable output is generally preferred in neuromuscular electrical stimulation, especially for FES, which aims at recovering meaningful movement functions. The stable force profiles with gradual increase and decrease, as shown in Figure 4B, are more predictable than the force profile with abrupt change in Figure 4A. The stable force profiles with gradual change are generated by electrical stimulation

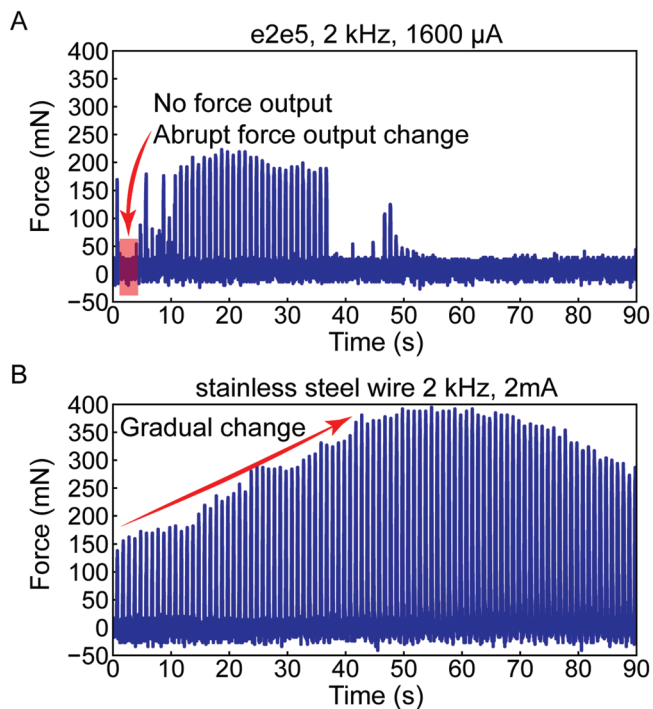


Figure 4. Force profiles measured from the same subject using different electrode sites. A) Force profile induced by e2 and e5 on the flexible intramuscular electrode shows abrupt increase and decrease. B) Force profile induced by two large-distance stainless steel wires is stable and shows gradual increase and decrease.

targeting at the end nerves, and such electrical stimulation induces slow disturbance on motoneuron excitability. To compare the properties of slow disturbance and fast disturbance, a circuit model is employed to simulate the voltage waveforms on the target motoneurons.

Figure 5A1 shows the circuit model to simulate voltage waveforms in response to electrical stimulation delivered by small-distance stimulation electrodes. In this circuit model, motoneurons are represented by RLC^[57–59] (resistor, inductor, and capacitor) components (green blocks P1–P4 in **Figure 5A1**). Muscle fibers are represented by RC^[60] (resistor and capacitor) components (blue blocks in **Figure 5A1**). In addition, extracellular medium is represented by pure resistors connecting the RC and RLC components. Here, two stimulation electrodes (E+ and E– in **Figure 5A1**) are chosen to represent the small-distance stimulation electrode pair. In this circuit modeling, current input is delivered from the two small-distance stimulation electrodes, and voltage waveforms are measured from motoneuron P1–P4, as shown in **Figure 5A2**. Similarly, the voltage waveforms generated by a large-distance electrode pair are modeled using the circuit model in **Figure 5B1**, and the voltage waveforms measured from motoneuron P1–P4 are shown in **Figure 5B2**. Here, the modeling of small-distance electrode pair in **Figure 5A1** is in correspondence to using the flexible intramuscular electrode, as the electrodes are close to the motoneurons. The modeling of large-distance electrode pair in **Figure 5B1** is in correspondence to using the stainless steel wires, as the stainless steel wires are further away from the motoneurons.

As shown in **Figure 5B2**, the voltage waveforms in response to electrical stimulation delivered by large-distance stimulation electrodes have two properties. First, when the current input is of the same amplitude, the amplitude of voltage waveforms in **Figure 5B2** is much smaller than that in **Figure 5A2**. Second, the voltage waveforms on P1 to P4 suffer from smaller spatial decay in **Figure 5B2** as compared to **Figure 5A2**. Considering these two properties, large-distance stimulation electrodes generate widely distributed small-amplitude stimulation over a large area, while small-distance stimulation electrodes induce localized large-amplitude stimulation over a small area. Thus, large-distance stimulation electrodes tend to induce slow disturbance on motoneuron excitability by targeting the widely distributed end nerves, which generates stable force output that meets the requirement of FES applications.

2.5. Characterization of Fast Disturbance on Motoneuron Excitability

To further investigate the properties of fast disturbance on motoneuron excitability, we compared positive-first and negative-first biphasic stimulation using the flexible intramuscular electrode on another subject. As shown in **Figure 6A1–A4**, the force profiles generated by positive-first stimulation show gradual change over the 90 s stimulation trials. However, in **Figure 6B1–B4**, the force profiles generated by negative-first stimulation show abrupt decrease and increase. Thus, when the flexible intramuscular electrode stimulates at the main nerve trunk, the induced fast disturbance on motoneuron excitability differs for positive-first and negative-first stimulation.

Figure 7 shows how positive-first and negative-first stimulation induce disturbance on motoneuron excitability differently. For both positive-first and negative-first biphasic stimulation, the negative current input opens the voltage-gated ion channels. In **Figure 7A1–A4**, voltage-gated ion channels will not open during the positive current input, and the orange curve indicated on the input current waveform does not generate action potentials. Only when the current input is negative, the ion channels will open. After the ion channels open, the unfinished negative current input (indicated by the blue curve on the input current waveform) overlaps with the generated action potential and distorts the natural ion redistribution. This unfinished negative current input hinders Na⁺ influx and facilitates K⁺ efflux, to increase the stimulation threshold, making the ion channels more difficult to open in the following stimulation. In this way, the opening of the ion channels gradually becomes later, and the overlap of the unfinished negative current input with the generated action potentials is shorter. This explains the gradual decrease of force profile in **Figure 6A1–A4**.

For negative-first biphasic stimulation, the ion channels open during the negative current input, as shown in **Figure 7B1–B4**. After the ion channels open, the unfinished negative current input and the following positive current input (indicated by the blue curve on the input current waveform) overlaps with generated action potential and distorts the natural ion redistribution. The disturbance induced by the positive stimulation is more prominent as compared to the negative stimulation, and the Na⁺ influx is facilitated and the K⁺ efflux is hindered, to decrease the

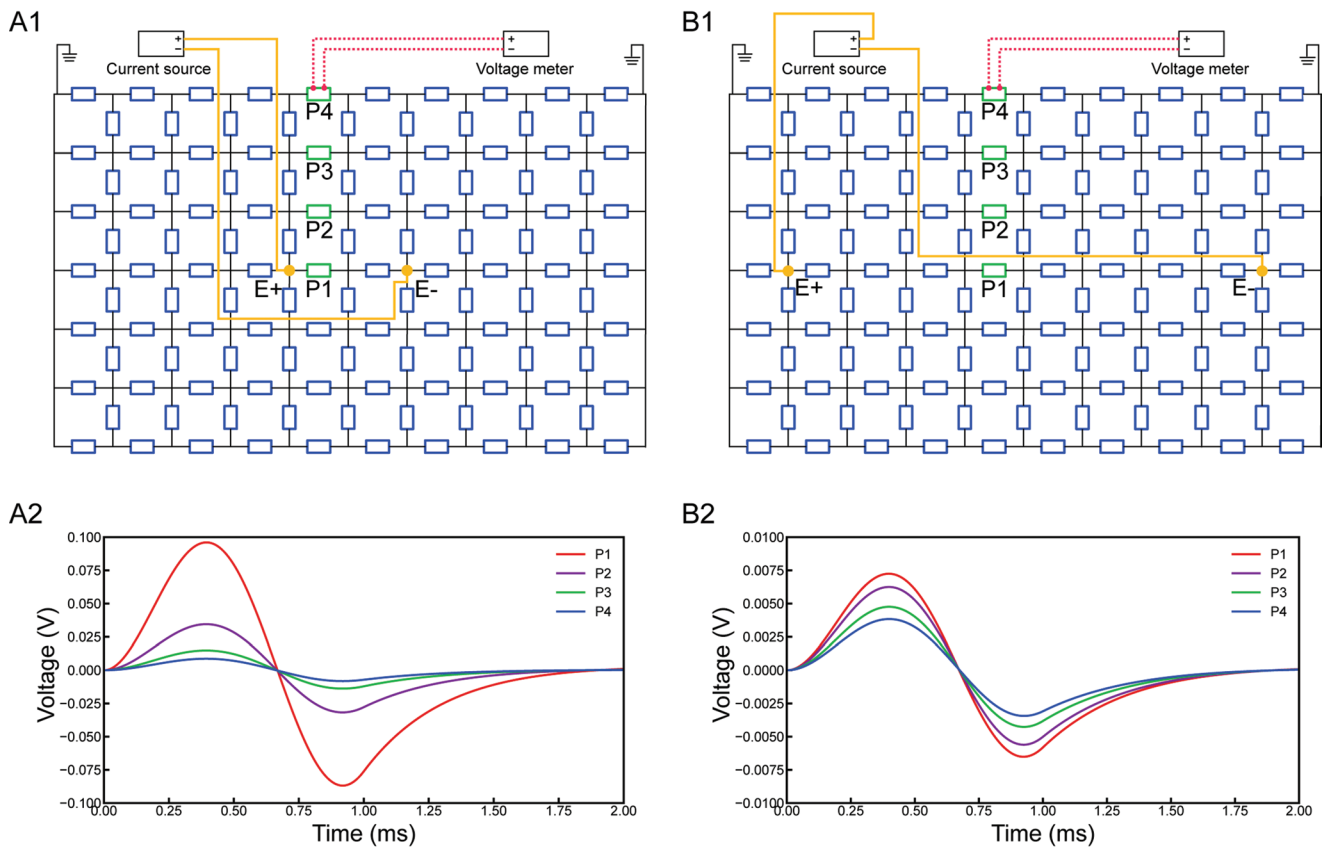


Figure 5. Large-distance stimulation electrodes tend to induce slow disturbance. A1) Distributed-parameter circuit model for small-distance electrodes. P1–P4 are RLC components (green blocks) representing target motoneurons. Blue blocks are RC components representing muscle fibers. E+ represents the electrode connected to positive terminal of the stimulator, and E− represents the electrode connected to negative terminal of the stimulator. A2) Voltage waveforms on P1–P4 as noted in (A1). B1) Distributed-parameter circuit model for large-distance electrodes. B2) Voltage waveforms on P1–P4 as noted in (B1).

stimulation threshold, making the ion channels easier to open in the following stimulation. Thus, the opening of the ion channels gradually becomes earlier. However, the accumulated Na^+ influx gradually decreases the transmembrane ion concentration, as shown in Figure 7C1–C4. The result is that although the threshold to open an ion channel is lower in Figure 7B4, the decreased transmembrane ion concentration cannot generate an action potential large enough to be transmitted. This explains the disappearance of force profile in Figure 6B1–B4.

3. Discussion

In this study, we find that the stimulation electrodes of different spatial arrangement with respect to the motoneuron distribution in the skeletal muscle induce different disturbance on motoneuron excitability. The short-distance stimulation electrode sites on the flexible intramuscular electrode target the main motor nerve trunk in the muscle tissue and induce fast disturbance on motoneuron excitability. The large-distance stainless-steel wires target the widely distributed end nerves in the muscle and exert slow disturbance on motoneuron excitability. We will discuss the potential applications for slow and fast disturbance in neuromodulation of muscle tissues.

In the case of slow disturbance, large-distance stimulation electrodes widely exert small-amplitude stimulation over a large area. As shown in Figure 4B, stable force profiles with gradual increase and decrease are generated. Although the way by which large-distance stimulation electrodes activate motoneurons is still different from the natural action potentials, the disturbance on motoneuron excitability is small. In this way, the motoneuron response to the same electrical stimulation will only slowly change, to show as stable force profile with gradual increase and decrease. Such stable output is desirable in FES, as the output is predictable when the input is fixed. To achieve constant force output when constant input is applied, close-loop control can be developed to compensate the slowly changing motoneuron excitability which is inevitably induced by electrical stimulation.

In the case of fast disturbance, short-distance stimulation electrodes induce synchronized large-amplitude disturbance on all the motoneurons in the main motor nerve trunk, to generate force output with abrupt increase and decrease, as shown in Figure 4A. Such force output with abrupt change is not suitable for FES, however, the disappearance of force output opens the possibility for muscle conduction block application. Nerve conduction block is widely applied to better control urine for bladder dysfunction treatment.^[61] Here, we

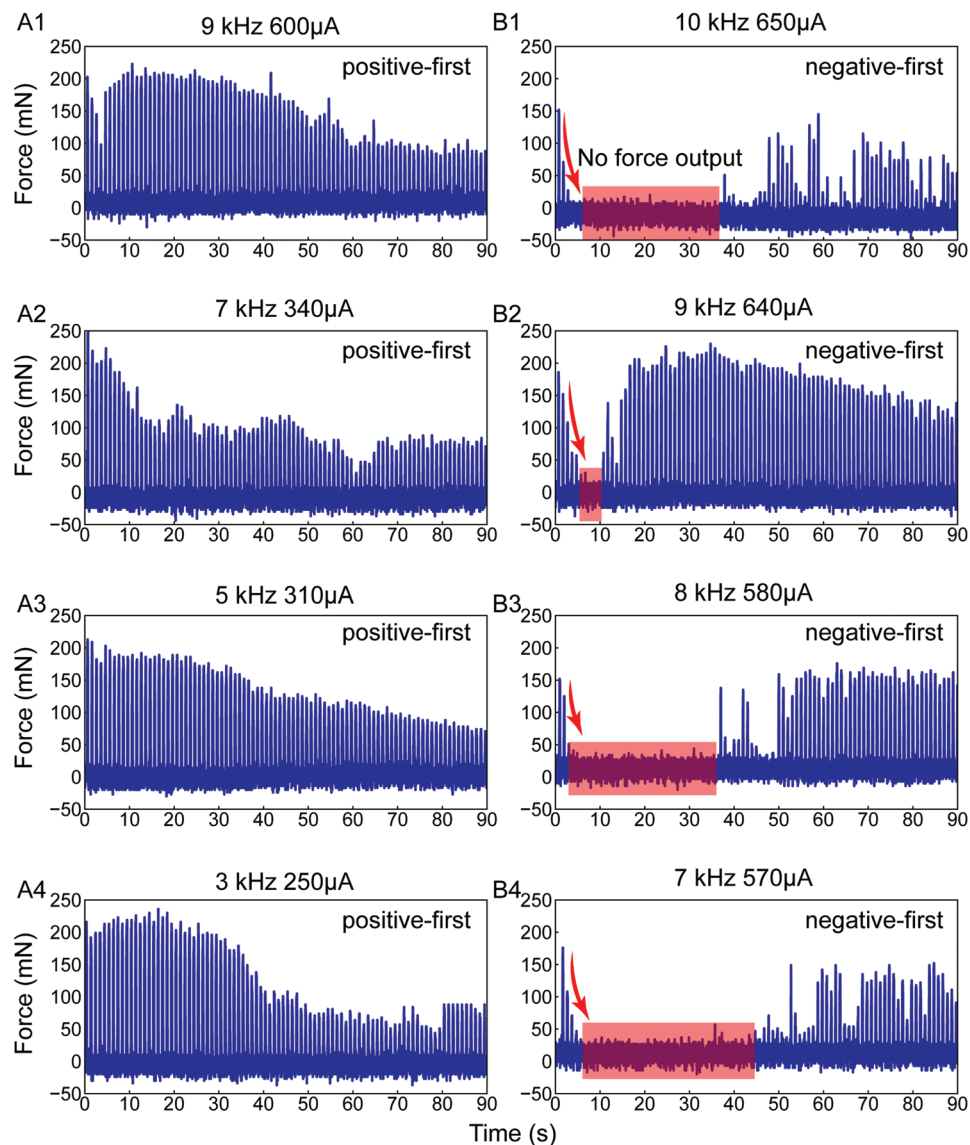


Figure 6. Fast disturbance on neuron excitability for various positive-first stimulation and negative-first stimulation. The force profiles were observed on the same subject. A1–A4) Positive-first stimulation induces force profile with gradual increase and decrease. B1–B4) Negative-first stimulation induces force profile with abrupt increase and decrease. The force profile masked in red shows zero force output.

have demonstrated that by targeting the main motor nerve trunk using the flexible intramuscular electrode, muscle conduction block can be induced by depleting the transmembrane ion concentration difference with fast disturbance. Such muscle conduction block can be potentially used for muscle spasticity treatment, which shows as involuntary muscle contractions. By artificially depleting the transmembrane ion concentration on the main motor nerve trunk, the muscle will not respond to the involuntary motor intentions, so that muscle spasticity can be relieved.

The novel flexible intramuscular electrode reported here enables exploration of different electrical stimulation strategies. By selectively stimulating the main motor nerve trunk or the widely distributed end motor nerves, control over dynamic or static neuron excitability can be realized. If this electrode

and the corresponding stimulation strategies are further combined with recently developed implantable energy-harvesting devices,^[62–64] a completely new self-powered rehabilitation system could potentially be realized.

4. Conclusion

We have demonstrated how a flexible multiple-channel intramuscular electrode can be used to explore various electrical control of the skeletal muscles. Here, we explore the spatial interaction between the stimulation electrodes and the tissue. We discover the phenomena of slow and fast disturbance when targeting at the main motor nerve trunk and the end motor nerves. Slow disturbance is induced by large-distance

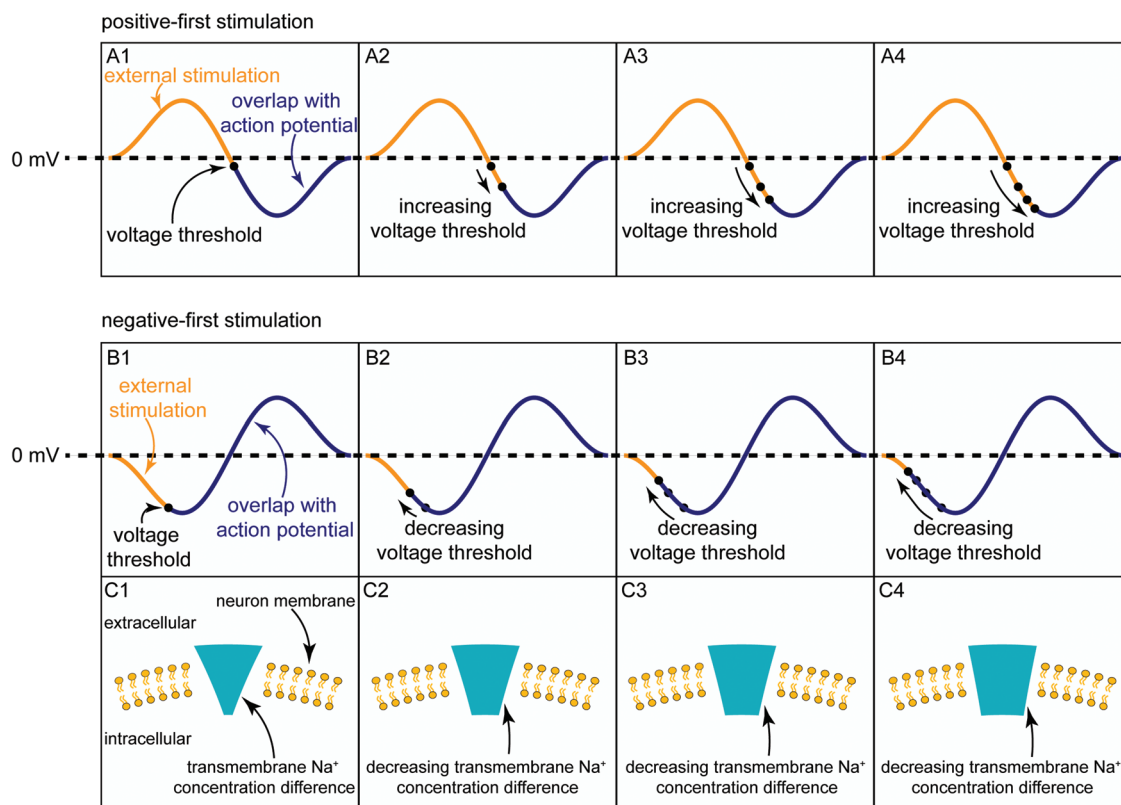


Figure 7. Illustration of how external stimulation dynamically shifts neuron excitability. A1–A4) Interaction between positive-first stimulation and action potentials. B1–B4) Interaction between negative-first stimulation and action potentials. C1–C4) Transmembrane Na^+ concentration difference decreases when the voltage threshold decreases in (B1–B4).

electrodes and generates force output with gradual change, which is suitable for FES applications. Fast disturbance is induced by small-distance electrodes and generates force output with abrupt change. The disappearance of force output by artificially depleting the transmembrane ion concentration difference opens the possibility for muscle conduction block application, which can be used for muscle spasticity treatment.

5. Experimental Section

In Vivo Experiment: All experiments were conducted according to protocols approved by the Institutional Animal Care and Use Committee at the National University of Singapore. Six Sprague-Dawley rats (around 450 g, female) were used for the acute experiments. Anesthesia was induced with isoflurane (Aerrane, Baxter Healthcare Corp., USA). Carprofen (Rimadyl, Zoetis, Inc., USA) was injected for pain relief before surgery. After the rat was anesthetized, fur on the leg was gently removed by a shaver. Then, the skin was disinfected with 70% ethanol wipes, and an incision was made with a surgical blade to expose the Tibialis Anterior (TA) muscle. The flexible intramuscular electrode and two stainless steel wires were sutured into the TA muscle. After the electrode implantation, the skin was sutured back.

The customized current stimulation waveform was generated by MATLAB (MathWorks, USA) to control a Data Acquisition device (DAQ, National Instruments, USA). The voltage output generated by the DAQ was connected to an isolated high-power stimulator (A-M SYSTEMS model 4100, USA), to generate current output to stimulate the TA muscle. The anesthetized rat was fixed on a stand, and the ankle of left leg was

connected to a dual-range force sensor (Vernier, USA). This force sensor was connected to a laptop through a DAQ. LabView (National Instruments, USA) was used for on-site result visualization during the measurements.

Circuit Modeling: The modeling was performed on MATLAB. First, a circuit description was performed in Simulink (MathWorks, USA). Then, current inputs of different waveforms were recursively fed to the circuit model, and the voltage responses of the targeted RLC component were collected. Finally, these voltage responses were fed into the probability equation to calculate the probability of neuron excitation under these current inputs.

Statistical Analysis: Analysis and visualization of the measured force data were performed using MATLAB. The raw measurement data were presented in this paper, without transformation or normalization.

Supporting Information

Supporting Information is available from the Wiley Online Library or from the author.

Acknowledgements

The authors thank Dr. Shih-Cheng Yen and Dr. Nitish V. Thakor for helpful discussions on the manuscript. This work was supported by the following grant from the National Research Foundation: Competitive Research Project ‘Peripheral Nerve Prostheses: A Paradigm Shift in Restoring Dexterous Limb Function’ (NRF-CRP10-2012-01), and the grant from the HIFES Seed Funding: ‘Hybrid Integration of Flexible Power Source and Pressure Sensors’ (R-263-501-012-133).

Conflict of Interest

The authors declare no conflict of interest.

Keywords

electrical stimulation, flexible electrodes, neuromodulation

Received: September 30, 2018

Revised: April 17, 2019

Published online:

- [1] Kenry, J. C. Yeo, C. T. Lim, *Microsyst. Nanoeng.* **2016**, *2*, 16043.
- [2] S. Choi, H. Lee, R. Ghaffari, T. Hyeon, D. H. Kim, *Adv. Mater.* **2016**, *28*, 4203.
- [3] G. Li, Y. Li, G. Chen, J. He, Y. Han, X. Wang, D. L. Kaplan, *Adv. Healthcare Mater.* **2015**, *4*, 1134.
- [4] J. M. Seitz, M. Durisin, J. Goldman, J. W. Drelich, *Adv. Healthcare Mater.* **2015**, *4*, 1915.
- [5] J. J. Green, J. H. Elisseeff, *Nature* **2016**, *540*, 386.
- [6] A. Chortos, J. Liu, Z. Bao, *Nat. Mater.* **2016**, *15*, 937.
- [7] T. Someya, Z. Bao, G. G. Malliaras, *Nature* **2016**, *540*, 379.
- [8] Y. S. Rim, S. H. Bae, H. Chen, N. De Marco, Y. Yang, *Adv. Mater.* **2016**, *28*, 4415.
- [9] Y. Zang, F. Zhang, C. A. Di, D. Zhu, *Mater. Horiz.* **2015**, *2*, 140.
- [10] X. Wang, L. Dong, H. Zhang, R. Yu, C. Pan, Z. L. Wang, *Adv. Sci.* **2015**, *2*, 1500169.
- [11] Y. Khan, A. E. Ostfeld, C. M. Lochner, A. Pierre, A. C. Arias, *Adv. Mater.* **2016**, *28*, 4373.
- [12] B. M. Quandt, L. J. Scherer, L. F. Boesel, M. Wolf, G. L. Bona, R. M. Rossi, *Adv. Healthcare Mater.* **2015**, *4*, 330.
- [13] S. Sugama, K. Sekiyama, T. Kodama, Y. Takamatsu, M. Hashimoto, C. Bruno, Y. Kakinuma, M. Systems, C. Biology, L. Jolla, *Sci. Transl. Med.* **2017**, *8*, 39.
- [14] D. J. Lipomi, M. Vosgueritchian, B. C. K. Tee, S. L. Hellstrom, J. A. Lee, C. H. Fox, Z. Bao, *Nat. Nanotechnol.* **2011**, *6*, 788.
- [15] B. C.-K. Tee, A. Chortos, A. Berndt, A. K. Nguyen, A. Tom, A. McGuire, Z. C. Lin, K. Tien, W.-G. Bae, H. Wang, P. Mei, H.-H. Chou, B. Cui, K. Deisseroth, T. N. Ng, Z. Bao, *Science* **2015**, *350*, 313.
- [16] T. Someya, T. Sekitani, S. Iba, Y. Kato, H. Kawaguchi, T. Sakurai, *Proc. Natl. Acad. Sci. U S A* **2004**, *101*, 9966.
- [17] J. Wang, in *Electrochemical Sensors, Biosensors and their Biomedical Applications*, First Edition (Eds: X. Zhang, H. Ju, J. Wang), Elsevier, Amsterdam, **2008**, pp. 57–69.
- [18] S. Lee, H. Wang, W. Y. Xian Peh, T. He, S.-C. Yen, N. V. Thakor, C. Lee, *Nano Energy* **2019**, *60*, 449.
- [19] S. Lee, C. Lee, *Curr. Opin. Biomed. Eng.* **2018**, *6*, 130.
- [20] L. Chen, Q. Shi, Y. Sun, T. Nguyen, C. Lee, S. Soh, *Adv. Mater.* **2018**, *30*, 1.
- [21] B. C. Knollmann, *Nat. Methods* **2010**, *7*, 889.
- [22] K. L. Montgomery, S. M. Iyer, A. J. Christensen, K. Deisseroth, S. L. Delp, *Sci. Transl. Med.* **2016**, *8*, 337rv5.
- [23] K. L. Montgomery, A. J. Yeh, J. S. Ho, V. Tsao, S. M. Iyer, L. Grosenick, E. A. Ferenczi, Y. Tanabe, K. Deisseroth, S. L. Delp, A. S. Y. Poon, *Nat. Methods* **2015**, *12*, 969.
- [24] C. J. Payne, I. Wamala, C. Abah, T. Thalhofer, M. Saeed, D. Bautista-Salinas, M. A. Horvath, N. V. Vasilyev, E. T. Roche, F. A. Pigula, C. J. Walsh, *Soft Rob.* **2017**, *4*, 241.
- [25] F. Arab Hassani, R. P. Mogan, G. G. L. Gammad, H. Wang, S. C. Yen, N. V. Thakor, C. Lee, *ACS Nano* **2018**, *12*, 3487.
- [26] H. Wang, G. Pastorin, C. Lee, *Adv. Sci.* **2016**, *3*, 1500441.
- [27] D. A. LaVan, T. McGuire, R. Langer, *Nat. Biotechnol.* **2003**, *21*, 1184.
- [28] M. Kogan, M. McGuire, J. Riley, *Neurosurg. Clin. North Am.* **2019**, *30*, 137.
- [29] C. Freeman, N. Ostle, H. Kang, *Nature* **2001**, *409*, 149.
- [30] S. Musallam, *Science* **2004**, *305*, 258.
- [31] P. Nair, *Proc. Natl. Acad. Sci. U S A* **2013**, *110*, 18343.
- [32] T. A. Asbeck, S. M. M. De Rossi, G. Ignacio, D. Ye, W. Conor, *IEEE Rob. Autom. Mag.* **2011**, *21*, 22.
- [33] Y. Ding, M. Kim, S. Kuindersma, C. J. Walsh, *Sci. Rob.* **2018**, *3*, eaar5438.
- [34] S. Lee, H. Wang, Q. Shi, L. Dhakar, J. Wang, N. V. Thakor, S.-C. Yen, C. Lee, *Nano Energy* **2017**, *33*, 1.
- [35] Q. Shi, T. He, C. Lee, *Nano Energy* **2019**, *57*, 851.
- [36] N. Kipnis, *Ann. Sci.* **1987**, *44*, 107.
- [37] V. R. Zschorlich, R. Köhling, *PLoS One* **2013**, *8*, e83845.
- [38] W. Catterall, *Science* **1988**, *242*, 50.
- [39] C. C. McIntyre, S. Mori, D. L. Sherman, N. V. Thakor, J. L. Vitek, *Clin. Neurophysiol.* **2004**, *115*, 589.
- [40] C. Ethier, E. R. Oby, M. J. Bauman, L. E. Miller, *Nature* **2012**, *485*, 368.
- [41] S. Raspopovic, M. Capogrosso, F. M. Petrini, M. Bonizzato, J. Rigosa, G. Di Pino, J. Carpaneto, M. Controzzi, T. Boretius, E. Fernandez, G. Granata, C. M. Oddo, L. Citi, A. L. Ciancio, C. Cipriani, M. C. Carozza, W. Jensen, E. Guglielmelli, T. Stieglitz, P. M. Rossini, S. Micera, *Sci. Transl. Med.* **2014**, *6*, 222ra19.
- [42] S. Lee, W. Y. X. Peh, J. Wang, F. Yang, J. S. Ho, N. V. Thakor, S. Yen, C. Lee, *Adv. Sci.* **2017**, *4*, 1700149.
- [43] J. Wang, Z. Xiang, G. Gerald, L. Gammad, N. V. Thakor, S. Yen, C. Lee, *Sens. Actuators, A* **2016**, *249*, 269.
- [44] I. Delgado-Martínez, J. Badia, A. Pascual-Font, A. Rodríguez-Baeza, X. Navarro, *Front. Neurosci.* **2016**, *10*, 286.
- [45] Z. Xiang, S. Sheshadri, S.-H. Lee, J. Wang, N. Xue, N. V. Thakor, S.-C. Yen, C. Lee, *Adv. Sci.* **2016**, *3*, 1500386.
- [46] Q. Xu, Y. Quan, L. Yang, J. He, *IEEE Trans. Neural Syst. Rehabil. Eng.* **2013**, *21*, 65.
- [47] M. P. Willand, C. D. Chiang, J. J. Zhang, S. W. P. Kemp, G. H. Borschel, T. Gordon, *Neurorehabilitation Neural Repair* **2015**, *29*, 690.
- [48] A. B. Ajiboye, F. R. Willett, D. R. Young, W. D. Mernberg, B. A. Murphy, J. P. Miller, B. L. Walter, J. A. Sweet, H. A. Hoyen, M. W. Keith, P. H. Peckham, J. D. Simeral, J. P. Donoghue, L. R. Hochberg, R. F. Kirsch, *Lancet* **2017**, *389*, 1821.
- [49] S. Musallam, B. D. Corneil, B. Greger, H. Scherberger, R. A. Andersen, *Science* **2004**, *305*, 258.
- [50] L. Guo, G. S. Guvanasen, X. Liu, C. Tuthill, T. R. Nichols, S. P. DeWeerth, *IEEE Trans. Biomed. Circ. Syst.* **2013**, *7*, 1.
- [51] D. H. Kim, J. Vimenti, J. J. Amsden, J. Xiao, L. Vigeland, Y. S. Kim, J. A. Blanco, B. Panilaitis, E. S. Frechette, D. Contreras, D. L. Kaplan, F. G. Omenetto, Y. Huang, K. C. Hwang, M. R. Zakin, B. Litt, J. A. Rogers, *Nat. Mater.* **2010**, *9*, 1.
- [52] L. Xu, S. R. Gutbrod, Y. Ma, A. Petrossians, Y. Liu, R. C. Webb, J. A. Fan, Z. Yang, R. Xu, J. J. Whalen, J. D. Weiland, Y. Huang, I. R. Efimov, J. A. Rogers, *Adv. Mater.* **2015**, *27*, 1730.
- [53] X. Wei, L. Luan, Z. Zhao, X. Li, H. Zhu, O. Potnis, C. Xie, *Adv. Sci.* **2018**, *5*, 1700625.
- [54] A. Kundu, K. R. Harreby, K. Yoshida, T. Boretius, T. Stieglitz, W. Jensen, *IEEE Trans. Neural Syst. Rehabil. Eng.* **2014**, *22*, 400.
- [55] J. R. Sanes, J. W. Lichtman, *Annu. Rev. Neurosci.* **1999**, *22*, 389.
- [56] K. Zhao, C. Shen, Y. Lu, Z. Huang, L. Li, C. D. Rand, J. Pan, X.-D. Sun, Z. Tan, H. Wang, G. Xing, Y. Cao, G. Hu, J. Zhou, W.-C. Xiong, L. Mei, *J. Neurosci.* **2017**, *37*, 3465.
- [57] B. Vazifehkhah Ghaffari, M. Kouhnavard, T. Aihara, T. Kitajima, *Biomed Res. Int.* **2015**, *2015*, 1.

- [58] A. Thomas, *J. Phys. D: Appl. Phys.* **2013**, *46*, 093001.
- [59] F. Wu, J. Ma, G. Zhang, *Appl. Math. Comput.* **2019**, *347*, 590.
- [60] C. Morris, H. Lecar, *Biophys. J.* **1981**, *35*, 193.
- [61] W. Y. X. Peh, R. Mogan, X. Y. Thow, S. M. Chua, A. Rusly, N. V. Thakor, S. C. Yen, *Front. Neurosci.* **2018**, *12*, 1.
- [62] Q. Zheng, Y. Zou, Y. Zhang, Z. Liu, B. Shi, X. Wang, Y. Jin, H. Ouyang, Z. Li, Z. L. Wang, *Sci. Adv.* **2016**, *2*, e1501478.
- [63] C. Sun, Q. Shi, D. Hasan, M. S. Yazici, M. Zhu, Y. Ma, B. Dong, Y. Liu, C. Lee, *Nano Energy* **2019**, *58*, 612.
- [64] B. Shi, Z. Li, Y. Fan, *Adv. Mater.* **2018**, *30*, e1801895.